

Indication of strong interatomic Coulombic decay in slow He^{2+} - Ne_2 collisions

Tom Kirchner*

*Department of Physics and Astronomy,
York University, Toronto, Ontario M3J 1P3, Canada*

(Dated: October 22, 2021)

Abstract

Electron removal in collisions of alpha particles with neon dimers is studied using an independent-atom-independent-electron model based on the semiclassical approximation of heavy-particle collision physics. The dimer is assumed to be frozen at its equilibrium bond length and collision events for the two ion-atom subsystems are combined in an impact parameter by impact parameter fashion for three mutually perpendicular orientations. Both frozen atomic target and dynamic response model calculations are carried out using the coupled-channel two-center basis generator method. We pay particular attention to inner-valence $\text{Ne}(2s)$ electron removal, which is associated with interatomic Coulombic decay (ICD), resulting in low-energy electron emission and dimer fragmentation. Our calculations confirm a previous experimental result at 150 keV/amu impact energy regarding the relative strength of ICD compared to direct electron emission. They further indicate that ICD is the dominant $\text{Ne}^+ + \text{Ne}^+$ fragmentation process below 10 keV/amu, suggesting that a strong low-energy electron yield will be observed in the ion-dimer system in a regime in which the creation of continuum electrons is a rare event in the ion-atom problem.

* tomk@yorku.ca

I. INTRODUCTION

The dominant reaction channel in low-energy ion-atom collisions is electron capture by the charged projectile. For example, in the He^{2+} -Ne system the cross section for net capture plateaus at a value on the order of 10^{-15} cm^2 at impact energies $E_P \approx 10 \text{ keV/amu}$, while that for direct transfer to the continuum is about an order of magnitude smaller and decreases rapidly toward lower E_P [1], i.e. it is exceedingly unlikely to find free electrons in this regime.

If the target atom happens to be in close proximity to another atom this may change, since a free-electron-producing channel that is non-existent in isolated atomic targets can open up: interatomic Coulombic decay (ICD). ICD involves the transfer of excitation energy, typically associated with the formation of a hole in an inner-valence orbital, from one atom to a neighboring one, and the release of that energy in the form of a low-energy continuum electron. The latter feature is of considerable applied relevance, since low-energy electrons are known to play an important role in numerous phenomena, most notably perhaps in inflicting damage in biological tissue [2].

ICD has been first observed in photoexcited noble gas clusters [3, 4], and has since been shown to occur in a variety of systems, including ion-impact collision problems at intermediate [5–7] and low E_P [8]. A number of review articles on ICD and its various forms have been published, among them [9] which focused on experimental studies and also discussed the relevance of ICD in biological systems, and, more recently, the comprehensive paper [10].

The observation of ICD in low-energy ion-impact collisions was perhaps somewhat surprising, given that the dominant capture processes usually involve outer-shell target electrons whose removal does not generate excitation energy in the ion left behind. In fact, in the experiments reported in [8] evidence for the occurrence of ICD was found in only one out of three collision systems studied, namely in $2.81 \text{ keV/amu O}^{3+}$ - Ne_2 collisions, while the kinetic energy release spectra obtained for $3.37 \text{ keV/amu Ar}^{9+}$ and $2.28 \text{ keV/amu Xe}^{20+}$ impact on Ne_2 suggested that ICD plays no appreciable role in these cases. Classical over-the-barrier model calculations published along with the data explained the absence of ICD for the Ar^{9+} and Xe^{20+} projectiles with strong $\text{Ne}(2p)$ capture happening simultaneously with and effectively overwhelming the inner-valence electron removal processes required to trigger ICD.

In a recent work using a similar model as in the present paper, we were able to confirm the occurrence of ICD for O^{3+} projectiles in a semi-quantitative fashion [11]. We further showed that the situation would be different and ICD very weak if bare triply-charged ions, i.e. Li^{3+} had been used in the experiment. This is so because the energy level structure of the bare projectile does not allow for efficient capture of a $Ne(2s)$ electron. Together with the findings of [8] this suggested that a delicate balance of charge state and structure of a projectile is required to make ICD a significant process. The question was raised if a projectile can be identified that maximizes the ICD yield in low-energy capture collisions [11].

The main objective of the present work is to report on a promising candidate: alpha particles, i.e. He^{2+} ions. Bare (and non-bare) helium ions were used in the experiments reported in [6, 7], but at higher impact energies $125 \text{ keV/amu} \leq E_P \leq 162.5 \text{ keV/amu}$, where direct target ionization competes with electron capture. ICD was successfully identified, but for most situations studied the direct electron emission yield was larger than the yield associated with ICD. We confirm this finding for He^{2+} collisions at $E_P = 150 \text{ keV/amu}$ and show that the situation is very different at $E_P \lesssim 10 \text{ keV/amu}$.

Our model is briefly summarized in Sec. II. For a more detailed discussion the reader is referred to our previous paper [11]. In Sec. III we present and discuss our results and in Sec. IV we offer a few concluding remarks.

II. MODEL

We work in the framework of the semiclassical approximation and assume that the projectile ion travels on a straight-line trajectory with constant speed $v = |\mathbf{v}|$. The neon dimer is assumed to remain fixed in space during the collision at its equilibrium bond length $R_e = 5.86 \text{ a.u.}$ [8, 12], and its interaction with the projectile is described as two independent ion-atom collisions occurring at impact parameters b^A and b^B which, depending on the relative orientation of the dimer with respect to the projectile velocity vector \mathbf{v} , may be the same or different. Three perpendicular orientations are considered: One in which the projectile travels parallel to the dimer axis such that $b^A = b^B = b$, where b is the impact parameter measured with respect to the center of mass of the dimer (orientation I), one in which the dimer is perpendicular to \mathbf{v} in the scattering plane defined by \mathbf{v} and \mathbf{b} (orientation II), and one in which the dimer is perpendicular to the scattering plane. Transition probabilities for

the ion-dimer system are calculated by combining probabilities for those ion-atom processes at b^A and b^B which correspond to a given process of interest j at the impact parameter b , and an orientation average is constructed for each j according to

$$P_j^{\text{ave}}(b) = \frac{1}{3} [P_j^{\text{I}}(b) + P_j^{\text{II}}(b) + P_j^{\text{III}}(b)]. \quad (1)$$

Orientation-averaged total cross sections are obtained by integration over the impact parameter

$$\sigma_j^{\text{ave}} = \int P_j^{\text{ave}}(b) d^2b = 2\pi \int_0^{b_{\text{max}}} b P_j^{\text{ave}}(b) db \quad (2)$$

with $b_{\text{max}} = 10$ a.u., which turned out to be sufficient to capture all appreciable contributions. We note that the same orientation-averaging procedure was used in numerous theoretical studies of collisions involving hydrogen molecules (see, e.g. [13, 14] and references therein).

The ion-atom collision calculations are carried out at the level of the independent electron model (IEM). We consider both a frozen target potential (no-response) model and a more sophisticated model which includes dynamic response following the prescription of [1]. The atomic neon potential used in both variants is obtained from an optimized potential method (OPM) calculation at the level of the exchange-only approximation [15]. The gist of the response model is to adjust the potential during the collision in a way that reflects the ionic character a target atom acquires when electrons are removed from it. The time-dependent net electron removal probability is used to regulate the ionic character such that response effects remain small as long as zero-fold and one-fold electron removal dominate, and become appreciable once higher-order removal processes contribute substantially [1]. The response model has been applied successfully to numerous ion-atom collision problems (see, e.g. [16–18] and references therein), but one should bear in mind that it deals in a global fashion with dynamic effects which ideally would be handled at a *microscopic* level, e.g. in a time-dependent OPM framework. The latter is challenging to implement for atoms with more than two electrons [19, 20] and is beyond the scope of the present work.

Following our previous work for triply-charged ion-dimer collisions [11] we assume the Ne K -shell electrons to be passive and solve the single-particle Schrödinger equations for the eight Ne L -shell electrons using the two-center basis generator method (TC-BGM). The basis sets used include the $2s$ to $4f$ target orbitals and (i) at impact energies $E_P \geq 20$ keV/amu all projectile orbitals from $1s$ to $4f$, and (ii) all projectile orbitals up to $7i$ at lower

E_P . We have checked at $E_P = 10$ keV/amu that including these additional projectile states result in insignificant changes except at impact parameters smaller than one atomic unit.

The bound-state two-center basis sets are augmented by pseudo states to account for couplings to the continuum using the standard BGM procedure of operating with powers of a regularized projectile potential operator on the target eigenstates [21]. For the low projectile energy calculations we included the same set of states as in [11], while at $E_P \geq 20$ keV/amu a significantly larger set of pseudo states, similar to the sets discussed in [17], was used in order to describe the increasing importance of transitions to the continuum with sufficient accuracy. The latter reference includes basis set convergence studies and also provides some details on the implementation of the dynamic response model of [1] within the TC-BGM.

The impact parameter by impact parameter combination of atomic results to assemble transition probabilities for the ion-dimer system is based on straightforward multinomial statistics involving products of single-electron transition probabilities, i.e. it is consistent with the IEM. We are not interested in a complete analysis including all conceivable removal processes of a total of N electrons, but focus on those which can be associated with the $\text{Ne}^+ + \text{Ne}^+$ fragmentation channel. These are (i) the removal of one $2p$ electron from each of the two neon atoms resulting in the direct production of the $\text{Ne}^+(2p^{-1}) + \text{Ne}^+(2p^{-1})$ configuration, (ii) the similar direct production of the $\text{Ne}^+(2s^{-1}) + \text{Ne}^+(2p^{-1})$ configuration, (iii) the direct production of $\text{Ne}^+(2s^{-1}) + \text{Ne}^+(2s^{-1})$, (iv) the removal of two $2p$ electrons from one of the two atoms while the other atom remains neutral, (v) the removal of one $2s$ electron from one of the two atoms while the other atom remains neutral. We will refer to processes (i) to (iii) as direct Coulomb explosion (CE) channels¹. Process (iv) leads to a transient state which can relax to the $\text{Ne}^+(2p^{-1}) + \text{Ne}^+(2p^{-1})$ configuration via radiative charge transfer (RCT) and process (v) corresponds to ICD [8, 11].

The explicit multinomial expressions for these processes are lengthy. For the first CE process and the processes associated with RCT and ICD they were given explicitly in [11] for orientation I. In this work we go one step further by separating all five processes in terms of transitions to bound projectile states (capture) and the continuum (ionization). As an example, let us consider the $2s$ -vacancy production process (v) associated with ICD. In

¹ Processes (ii) and (iii) generate some excitation energy in one or both atoms, but not enough to ionize an additional electron of the dimer, i.e. they cannot trigger ICD.

orientation I in which $b_A = b_B = b$ the probability for this process is

$$P_{2s-1}^x(b) = 4p_{2s}^x(b)[1 - p_{2s}^{\text{rem}}(b)]^3[1 - p_{2p_0}^{\text{rem}}(b)]^4[1 - p_{2p_1}^{\text{rem}}(b)]^8, \quad (3)$$

where p_{2s}^x is the single-particle probability for $x = \text{capture}$ or $x = \text{ionization}$ from the $2s$ initial state, and p_i^{rem} denote the single-particle removal probabilities from the $i = \{2s, 2p_0, 2p_1\}$ states. The factor of four reflects the fact that each of the four $2s$ electrons of the dimer can be the one that is captured or ionized and the $(1 - p_i^{\text{rem}})$ terms ensure that none of the other electrons is removed in the same event. Note that due to the symmetry of the ion-atom problem with respect to reflections about the scattering plane the probabilities for the $2p_{+1}$ and $2p_{-1}$ initial states are the same. The separation into capture and ionization events allows us to estimate the ratio of electron emission due to ICD compared to direct emission which was measured in [7] at $E_P = 150 \text{ keV/amu}$.

III. RESULTS AND DISCUSSION

We begin the discussion of results with a look at the atomic single-particle removal probabilities obtained in both no-response and response models. Figure 1 shows these probabilities at $E_P = 10 \text{ keV/amu}$ in panel (a) and at $E_P = 150 \text{ keV/amu}$ in panel (b). The current results are consistent with our earlier He^{2+} -Ne calculations reported in [1, 17, 22] (not shown).

Response effects are significant, particularly at the lower energy where electron capture to the projectile ground state is the dominant removal process. Only at relatively large impact parameters where all single-particle removal probabilities tend to be small do the no-response and response results merge. At $E_P = 10 \text{ keV/amu}$ removal from the $\text{Ne}(2s)$ initial state is very strong, particularly in the no-response model. This is due to the closeness of the single-particle energy eigenvalues of the initial ($\varepsilon_{\text{Ne}(2s)}^{\text{OPM}} = -1.718 \text{ a.u.}$) and final ($\varepsilon_{\text{He}^+(1s)} = -2 \text{ a.u.}$) states and their associated coupling. Dynamic response appears to weaken this coupling somewhat. The initial $\text{Ne}(2p)$ electrons are less likely to be captured because they are energetically farther away ($\varepsilon_{\text{Ne}(2p)}^{\text{OPM}} = -0.851 \text{ a.u.}$).

At $E_P = 150 \text{ keV/amu}$ transitions to the continuum dominate and the no response vs. response comparison mostly reflects the fact that ionization becomes less likely with increasing binding energy. The latter is also the reason why the $2p$ removal probabilities are larger than the $2s$ probability.

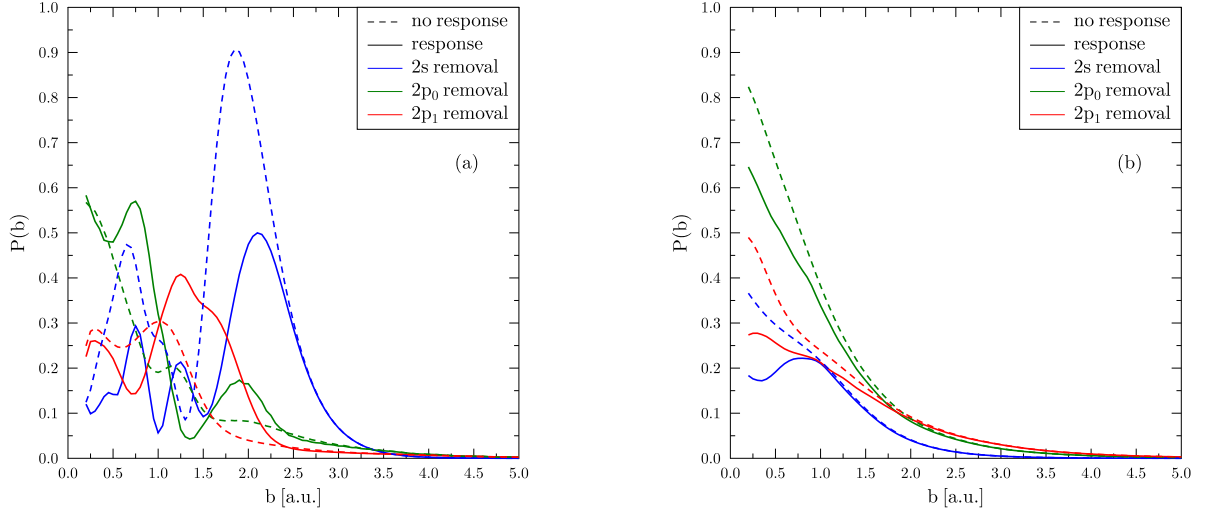


FIG. 1. Single-particle probabilities for electron removal from the Ne L shell by (a) $E_P = 10$ keV/amu and (b) $E_P = 150$ keV/amu He^{2+} impact plotted as functions of the impact parameter.

Figure 2 illustrates for orientation I in which the impact parameters of the atomic and the dimer problems are the same, how the single-particle probabilities shown in figure 1 translate into the dimer removal probabilities of interest in this work. At $E_P = 10$ keV/amu the main peak of the $2s$ -vacancy production channel associated with ICD (denoted by $2s^{-1}$ and shown in blue in figure 2) is almost the same in the no-response and response models despite the seemingly different single-particle $2s$ -removal probabilities. However, the $2s^{-1}$ peak occurs at $b = 2.6$ a.u., which is where the single-particle response and no-response probabilities shown in figure 1(a) begin to merge. They are strikingly different at smaller b and this is indeed reflected by larger differences in the $2s^{-1}$ data of figure 2(a). Somewhat counterintuitively, the strong no-response $2s$ -removal probability at $b \approx 1.9$ a.u. (figure 1(a)) is associated with a close-to-zero $2s^{-1}$ probability of the dimer (figure 2(a)). This is a consequence of the multinomial analysis in which the production of exactly one vacancy in a given subshell is associated with a product of one single-particle probability for the removal of an electron and $N - 1$ single-particle probabilities for not removing the other electrons (cf. equation (3)). The latter are very efficient suppression factors.

Clearly, the $2s$ -removal process associated with ICD is the strongest channel at $E = 10$

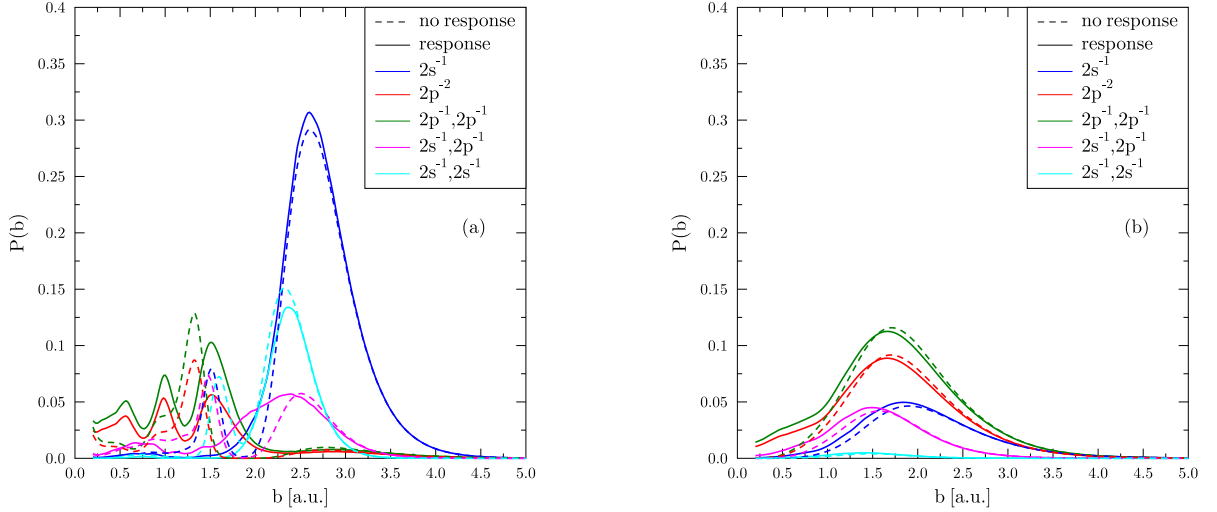


FIG. 2. Probabilities for $2s^{-1}$, $2p^{-2}$, $(2p^{-1}, 2p^{-1})$, $(2s^{-1}, 2p^{-1})$, and $(2s^{-1}, 2s^{-1})$ production at (a) $E_P = 10$ keV/amu and (b) $E_P = 150$ keV/amu in He^{2+} - Ne_2 collisions in orientation I, in which the projectile beam axis is parallel to the dimer axis, plotted as functions of the impact parameter.

keV/amu. The other two processes involving $2s$ removal (shown in magenta and cyan) are appreciable as well with their main peaks occurring in the $b = 2.3 - 2.5$ a.u. region. The processes involving the removal of two or one $2p$ electrons from one or both atoms (denoted by $2p^{-2}$ and $(2p^{-1}, 2p^{-1})$ in the figure) are mostly restricted to smaller impact parameters, which is not surprising given the structure of the single-particle probabilities shown in figure 1(a).

At $E = 150$ keV/amu the situation is quite different. In this case the $(2p^{-1}, 2p^{-1})$ and $2p^{-2}$ processes dominate, while the probabilities for the two processes involving the removal of one $2s$ electron are smaller and overall of similar strength, and the process involving the removal of two $2s$ electrons is very weak. All five probability curves display similar shapes as functions of b which is a direct consequence of the (mostly) monotonically decreasing behavior of the single-particle probabilities of figure 1(b). Effects due to dynamic response are minor at this energy except for the $2p$ removal processes at small b .

As demonstrated in [11] for triply-charged ion impact, the impact parameter dependences are markedly different for the other two orientations. Orientation III in which the dimer is

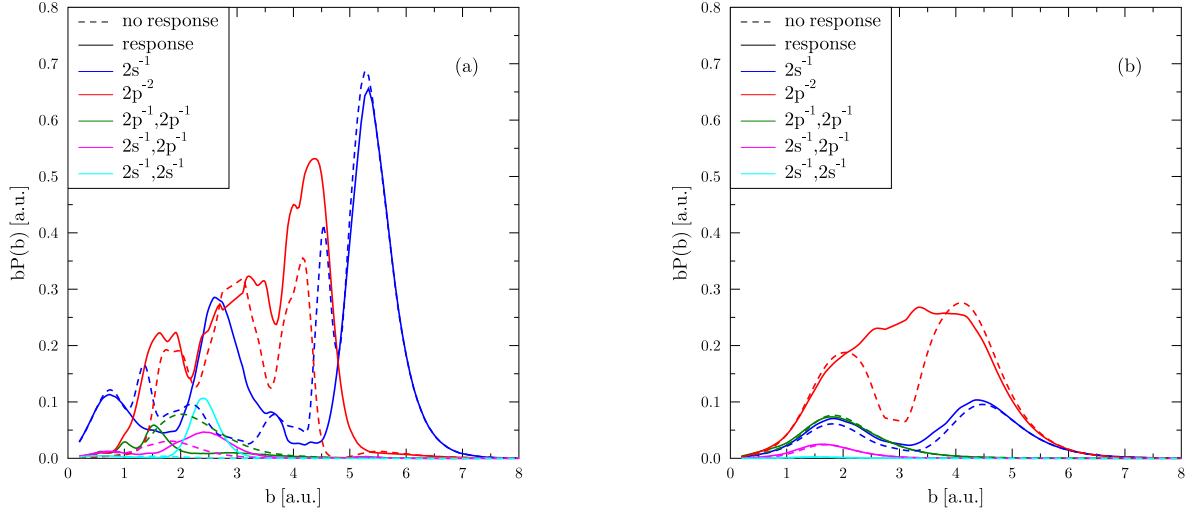


FIG. 3. Orientation-averaged impact-parameter-weighted probabilities for $2s^{-1}$, $2p^{-2}$, $(2p^{-1}, 2p^{-1})$, $(2s^{-1}, 2p^{-1})$, and $(2s^{-1}, 2s^{-1})$ production at (a) $E_P = 10$ keV/amu and (b) $E_P = 150$ keV/amu in He^{2+} - Ne_2 collisions plotted as functions of the impact parameter.

perpendicular to the scattering plane shows mostly small probabilities since the projectile does not get close enough to either neon atom to cause significant electron removal except at small b . In orientation II, by contrast, small impact parameter and even head-on ion-atom collisions contribute and may result in strong $2p$ electron removal around $b \approx R_e/2 = 2.93$ a.u. Similarly, for $2s$ vacancy production at $E_P = 10$ keV/amu the peak that appears at an impact parameter of 2.6 a.u. in orientation I is effectively moved to the impact parameter $b = 2.6$ a.u. $+ R_e/2 \approx 5.5$ a.u. in orientation II.

Figure 3 shows how this all adds up to the orientation-averaged probabilities for the processes of interest. In contrast to the previous plots the probabilities shown here are multiplied by the impact parameter such that the areas under the curves are directly proportional to the total cross sections (cf. equation (2)). At $E_P = 10$ keV/amu, the $2s^{-1}$ channel is the strongest process in the no-response model and overall about equally strong as the $2p^{-2}$ channel when dynamic response is included. The other three channels are significantly weaker. At $E_P = 150$ keV/amu the $2p^{-2}$ process prevails in both models. It is stronger in the dynamic response compared to the no-response model due to contributions

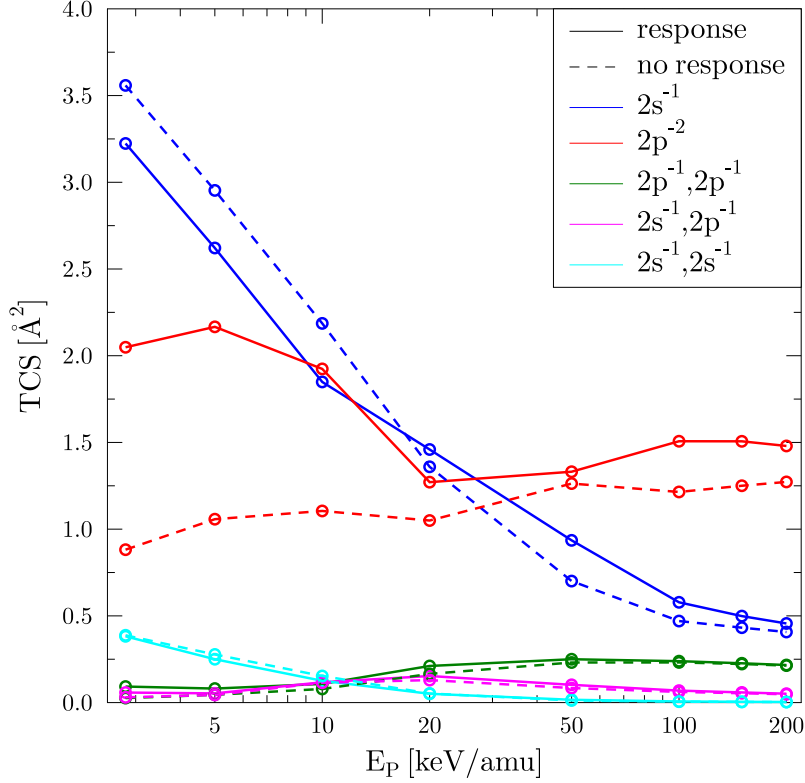


FIG. 4. Orientation-averaged total cross sections for $2s^{-1}$, $2p^{-2}$, $(2p^{-1}, 2p^{-1})$, $(2s^{-1}, 2p^{-1})$, and $(2s^{-1}, 2s^{-1})$ production in He^{2+} - Ne_2 collisions plotted as functions of the impact energy.

around $b = R_e/2$ which originate from close collisions with one of the neon atoms. The other channels only show small response effects.

Figure 4 displays the corresponding total cross sections. Response effects appear to be strongest for the $2p^{-2}$ channel, particularly at low energies where electron capture dominates. To understand the role of response we recall that (i) in this channel two electrons are removed from one atom, while the other channels involve at most one-electron removal per atom, and (ii) the response model is designed such that its effects become appreciable when more than one electron (on average) is removed from an atom.

Regardless of whether the no-response or response models are used, the $2s$ -vacancy production channel associated with ICD is the strongest process in low-velocity collisions. The

lowest energy we consider is $E_P = 2.81$ keV/amu, which is the energy that was used in the O^{3+} -Ne₂ experiment reported in [8]. In that experiment ICD was found to contribute 20% to the total $Ne^+ + Ne^+$ yield, while CE and RCT accounted for 10% and 70%, respectively. If we follow that work and assume that the $2p^{-2}$ channel leads to RCT in only 50% of all instances², while single $2s$ -vacancy production is always followed by ICD³, we obtain for the He^{2+} -Ne₂ system at $E_P = 2.81$ keV/amu the breakdowns 80:10:10 and 67:11:21 for ICD vs. CE vs. RCT in the no-response and response models, respectively, i.e. a remarkably strong ICD yield which should be easily identifiable in an experimental kinetic energy release spectrum.

Our results further indicate that ICD remains appreciable (and measurable) toward higher energies, although RCT takes over as the dominant channel and CE becomes slightly stronger on a relative scale. ICD was experimentally identified at $E_P = 150$ keV/amu in [7], but the relative yields of the three channels were not reported in that work. Instead, ejected electron spectra were shown for certain channels, and ratios of ICD vs. direct electron yields extracted from them. To make contact with those measurements we separate capture and ionization events and show in figure 5(a) and 5(b) respectively the partial cross sections that correspond to finding one electron in the continuum and one electron at the projectile after the collision (transfer ionization) and to finding two electrons in the continuum (double ionization). Note that for the $2s^{-1}$ channel we simply look at capture of one $2s$ electron and ionization of one $2s$ electron (cf. equation (3)) for the transfer ionization and double ionization channels respectively, since our formalism does not describe the ICD continuum electron explicitly. The plots are terminated at $E_P = 10$ keV/amu since the capture vs. ionization separation becomes inaccurate at lower energies where ionization is very small, and are shown on linear scales.

The transfer-ionization channel which corresponds to observing singly-charged projectiles after the collision is the one that was considered in [7] at $E_P = 150$ keV/amu. We observe in figure 5(a) that the $2s$ -vacancy production channel has a different shape compared to the others since it does not involve collisional ionization, but the capture of exactly one $2s$ electron. Accordingly, the $2s^{-1}$ process is much stronger than the other processes at low

² Two-electron removal from one of the two neon atoms does not have to be followed by RCT, but can also result in $Ne^{2+} + Ne$ fragmentation. Since the branching fractions of both decay modes are unknown, it seems natural to assume a 50:50 breakdown (see also the analysis presented in [23]).

³ ICD in small neon clusters was shown to be at least three orders of magnitude faster than de-excitation via photon emission [24] (see also the discussion in section 4 of the topical review article [9]).

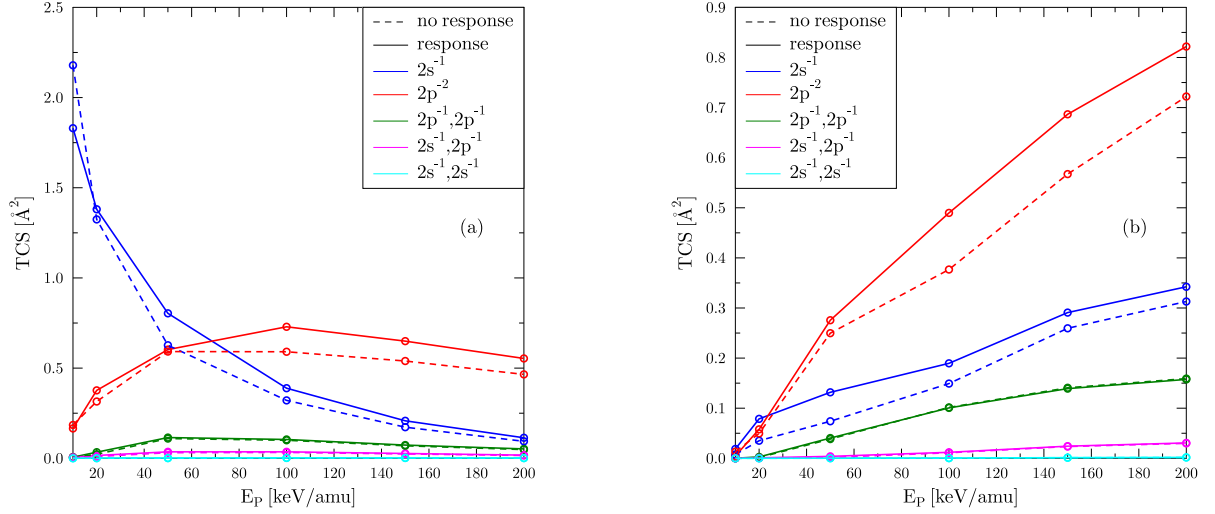


FIG. 5. Orientation-averaged total cross sections for $2s^{-1}$, $2p^{-2}$, $(2p^{-1}, 2p^{-1})$, $(2s^{-1}, 2p^{-1})$, and $(2s^{-1}, 2s^{-1})$ production in He^{2+} - Ne_2 collisions plotted as functions of the impact energy for the (a) transfer ionization channel, (b) double ionization channel (see text for details).

impact energies, but decreases with increasing energy and crosses the $2p^{-2}$ process. For the double ionization channel shown in figure 5(b) the shapes of all cross section curves are similar (monotonically increasing), which reflects the impact-energy dependence of pure ionization in the energy range considered. The removal of two $2p$ electrons from one atom ($2p^{-2}$) is the strongest process except perhaps at the lowest energies where all pure-ionization processes are weak.

Figure 6 shows the cross section ratio of the $2s^{-1}$ process compared to the sum of all other processes in the transfer-ionization channel. This should correspond to the ratio of the total ICD electron yield compared to the yield of directly ionized electrons for singly-charged helium ions in the final channel which was measured in [7]. Accordingly, that single experimental data point is included in the figure (using a red full circle). For both no-response and response models upper and lower bounds of the ratio are displayed, where the upper bound is obtained from the above-mentioned assumption that 50% of the $2p^{-2}$ events result in RCT and the lower bound from a more extreme 100% assumption. Response effects are rather small for this ratio and the experimental data point sits right in the middle

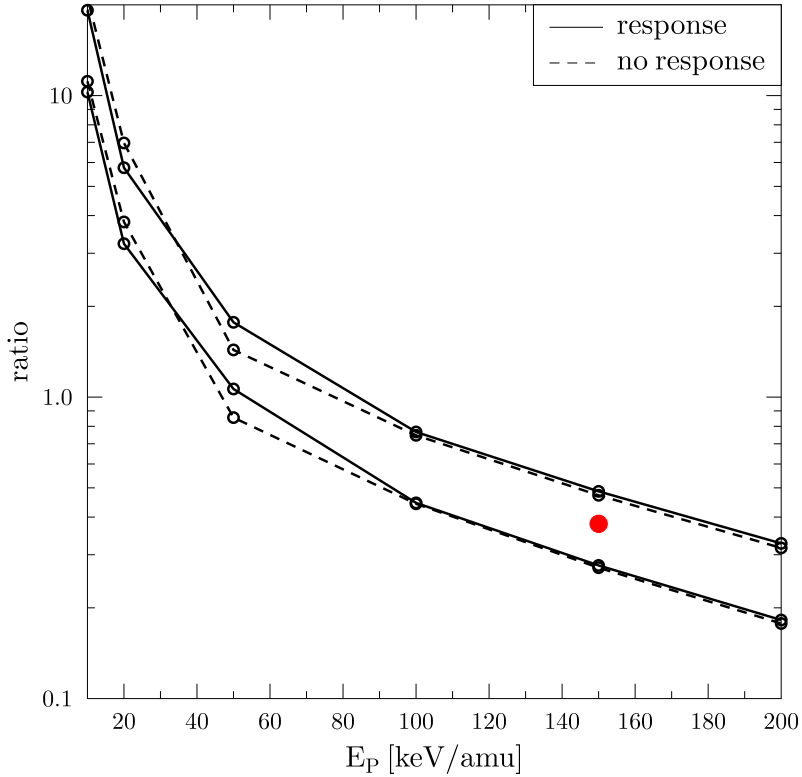


FIG. 6. Cross section ratio of the $2s^{-1}$ process compared to the other four processes included in figure 5(a) plotted as a function of the impact energy. The lines depict upper and lower bounds obtained by weighing the $2p^{-2}$ cross section with a factor of 0.5 and 1.0, respectively (see text for further explanation). Red bullet: experimental data point from [7] for the ratio of the electron yields due to ICD and direct ionization in the transfer ionization channel.

between the upper and lower bounds (at a value of 0.38). As can be inferred from figure 5(a) the ratio increases to large values between 10 and 20 toward the lowest energies considered. Once again, this indicates that ICD should be easily detectable in a low-energy measurement.

IV. CONCLUDING REMARKS

We have studied the one-electron and two-electron processes which are associated with ICD, CE, and RCT in the $\text{Ne}^+ + \text{Ne}^+$ fragmentation channel in He^{2+} - Ne_2 collisions. The calculations are at the level of an independent-atom-independent-electron model of the neon dimer, and the coupled-channel TC-BGM was used to propagate the initially populated orbitals in the field of the projectile potential. In contrast to a previous work for triply-charged projectile ions [11], both dynamic response and frozen-potential (no-response) calculations were carried out, and appreciable differences of both were found, in particular at low projectile energy. This raises the question if the previous (frozen potential) results for O^{3+} ion impact, which showed good agreement with available measurements, would be altered by response effects as well. A quantitative answer is not straightforward since the presence of electrons on the projectile complicates the situation for O^{3+} impact. However, two sets of test calculations using slightly different assumptions for the response potential both indicate that the effects of response are minor for the relative yields reported in [11]. Similarly, the relative yields for the $(2s^{-1}, 2p^{-1})$ and $(2s^{-1}, 2s^{-1})$ processes which were not considered in [11] turn out to be very small, i.e. neither item changes the conclusions of that work.

Coming back to the He^{2+} - Ne_2 system studied in the present work, our main results and conclusions can be summarized as follows:

(i) Given the simplicity of the response model and the fact that our theoretical description has other limitations as well (see below), we are not in a position to conclude that the response results are necessarily more accurate than the no-response results. Rather, the discrepancies between both sets of calculations should perhaps be interpreted more conservatively as an estimate of the theoretical model uncertainties [25]. Naturally, additional experimental data would help with a more definitive assessment of the response vs. no-response results reported here.

(ii) New experimental data may also help assess other limitations of our theoretical description [11], particularly those associated with the independent-atom-independent-electron model. For example, within this model the dynamical description of the ion-dimer collision does not take into account that the projectile charge state changes when an electron is captured from one of the two neon dimer atoms and that this change may affect the interaction of the projectile with the other atom. Another process which is ignored is the ion-impact-

induced ionization of one of the atoms and the subsequent ionization of the other one by a collision with the just released electron. An estimate using a model described in [26] suggests that the latter process results in a double ionization cross section of at most similar magnitude as the cross section for $(2s^{-1}, 2p^{-1})$ production shown in figure 5(b), and it obviously cannot affect the outcome in the transfer ionization channel shown in figure 5(a). It is more difficult to estimate the former limitation, i.e. effects of a dynamically changing projectile charge state on the transfer ionization results. Based on experience gathered from ion-atom collision studies one may argue that single-capture processes might be less affected than double-capture events [17], but ultimately this can only be decided by future calculations which take these effects into account.

(iii) With the caveat of the aforementioned model limitations the main finding of the present work is that single $2s$ -vacancy production is the strongest process at low impact energy, and, consequently, ICD the dominant $\text{Ne}^+ + \text{Ne}^+$ fragmentation channel in this region. This is a remarkable prediction in that it suggests that a large free electron yield will be observed in the ion-dimer system at collision energies where free-electron production is a very weak process in the ion-atom problem.

(iv) Key to the dominant role of ICD is strong $\text{Ne}(2s)$ capture with little simultaneous $\text{Ne}(2p)$ removal. Certainly, the He^{2+} -Ne system will not be unique in this regard, but it appears likely that this feature is more an exception than the rule for an ion-atom collision problem. Low-energy collisions are better candidates for giving rise to strong ICD than collisions at higher energies, since the latter are dominated by ionization processes which typically increase in strength with decreasing binding energy, i.e. strong inner-valence electron removal will be accompanied by even stronger outer-shell electron removal in this regime, effectively suppressing ICD.

Given the continuing interest in ICD it is hoped that this work will stimulate further experimental studies of this process in ion-impact collision problems. The comparison of accurate measurements and calculations can also shed light on the question of which fraction of two-electron removal from one atom (i.e. the $2p^{-2}$ process) gives rise to RCT. Our present and previous results for He^{2+} and O^{3+} collisions suggest that this fraction may be higher than 50%, and some of the over-the-barrier model calculations reported in [23] seem to suggest the same, but a more definitive answer is outstanding.

ACKNOWLEDGMENTS

Financial support from the Natural Sciences and Engineering Research Council of Canada (NSERC) (RGPIN-2019-06305) is gratefully acknowledged.

- [1] T. Kirchner, M. Horbatsch, H. J. Lüdde, and R. M. Dreizler, *Phys. Rev. A* **62**, 042704 (2000).
- [2] B. Boudaïffa, P. Cloutier, D. Hunting, M. A. Huels, and L. Sanche, *Science* **287**, 1658 (2000), <http://www.sciencemag.org/content/287/5458/1658.full.pdf>.
- [3] S. Marburger, O. Kugeler, U. Hergenhahn, and T. Möller, *Phys. Rev. Lett.* **90**, 203401 (2003).
- [4] T. Jahnke, A. Czasch, M. S. Schöffler, S. Schössler, A. Knapp, M. Kász, J. Titze, C. Wimmer, K. Kreidi, R. E. Grisenti, A. Staudte, O. Jagutzki, U. Hergenhahn, H. Schmidt-Böcking, and R. Dörner, *Phys. Rev. Lett.* **93**, 163401 (2004).
- [5] J. Titze, M. S. Schöffler, H.-K. Kim, F. Trinter, M. Waitz, J. Voigtsberger, N. Neumann, B. Ulrich, K. Kreidi, R. Wallauer, M. Odenweller, T. Havermeier, S. Schössler, M. Meckel, L. Foucar, T. Jahnke, A. Czasch, L. P. H. Schmidt, O. Jagutzki, R. E. Grisenti, H. Schmidt-Böcking, H. J. Lüdde, and R. Dörner, *Phys. Rev. Lett.* **106**, 033201 (2011).
- [6] H.-K. Kim, J. Titze, M. Schöffler, F. Trinter, M. Waitz, J. Voigtsberger, H. Sann, M. Meckel, C. Stuck, U. Lenz, M. Odenweller, N. Neumann, S. Schössler, K. Ullmann-Pfleger, B. Ulrich, R. C. Fraga, N. Petridis, D. Metz, A. Jung, R. Grisenti, A. Czasch, O. Jagutzki, L. Schmidt, T. Jahnke, H. Schmidt-Böcking, and R. Dörner, *Proceedings of the National Academy of Sciences* **108**, 11821 (2011), <https://www.pnas.org/content/108/29/11821.full.pdf>.
- [7] H.-K. Kim, H. Gassert, M. S. Schöffler, J. N. Titze, M. Waitz, J. Voigtsberger, F. Trinter, J. Becht, A. Kalinin, N. Neumann, C. Zhou, L. P. H. Schmidt, O. Jagutzki, A. Czasch, H. Merabet, H. Schmidt-Böcking, T. Jahnke, A. Cassimi, and R. Dörner, *Phys. Rev. A* **88**, 042707 (2013).
- [8] W. Iskandar, J. Matsumoto, A. Leredde, X. Fléchar, B. Gervais, S. Guillous, D. Hennecart, A. Méry, J. Rangama, C. L. Zhou, H. Shiromaru, and A. Cassimi, *Phys. Rev. Lett.* **114**, 033201 (2015).
- [9] T. Jahnke, *J. Phys. B: At. Mol. Opt. Phys.* **48**, 082001 (2015).

- [10] T. Jahnke, U. Hergenhahn, B. Winter, R. Dörner, U. Fröhling, P. V. Demekhin, K. Gokhberg, L. S. Cederbaum, A. Ehresmann, A. Knie, and A. Dreuw, *Chemical Reviews* **120**, 11295 (2020), pMID: 33035051, <https://doi.org/10.1021/acs.chemrev.0c00106>.
- [11] D. Bhattacharya and T. Kirchner, *Phys. Rev. A* **102**, 062816 (2020).
- [12] S. M. Cybulski and R. R. Toczyłowski, *J. Chem. Phys.* **111**, 10520 (1999).
- [13] A. Lühr and A. Saenz, *Phys. Rev. A* **81**, 010701 (2010).
- [14] Y. W. Zhang, J. W. Gao, Y. Wu, F. Y. Zhou, J. G. Wang, N. Sisourat, and A. Dubois, *Phys. Rev. A* **102**, 022814 (2020).
- [15] E. Engel and S. H. Vosko, *Phys. Rev. A* **47**, 2800 (1993).
- [16] T. Kirchner, H. J. Lüdde, and M. Horbatsch, *Recent Res. Dev. Phys.* **5**, 433 (2004).
- [17] G. Schenk and T. Kirchner, *Phys. Rev. A* **91**, 052712 (2015).
- [18] A. C. K. Leung and T. Kirchner, *Phys. Rev. A* **95**, 042703 (2017).
- [19] M. Keim, A. Achenbach, H. J. Lüdde, and T. Kirchner, *Phys. Rev. A* **67**, 062711 (2003).
- [20] M. Baxter, T. Kirchner, and E. Engel, *Phys. Rev. A* **96**, 032708 (2017).
- [21] M. Zapukhlyak, T. Kirchner, H. J. Lüdde, S. Knoop, R. Morgenstern, and R. Hoekstra, *J. Phys. B* **38**, 2353 (2005).
- [22] T. Kirchner, L. Gulyás, H. J. Lüdde, E. Engel, and R. M. Dreizler, *Phys. Rev. A* **58**, 2063 (1998).
- [23] W. Iskandar, X. Fléchar, J. Matsumoto, A. Leredde, S. Guillous, D. Hennecart, J. Rangama, A. Méry, B. Gervais, H. Shiromaru, and A. Cassimi, *Phys. Rev. A* **98**, 012701 (2018).
- [24] R. Santra, J. Zobeley, and L. S. Cederbaum, *Phys. Rev. B* **64**, 245104 (2001).
- [25] H.-K. Chung, B. J. Braams, K. Bartschat, A. G. Császár, G. W. F. Drake, T. Kirchner, V. Kokoouline, and J. Tennyson, *Journal of Physics D: Applied Physics* **49**, 363002 (2016).
- [26] B. Najjari, Z. Wang, and A. B. Voitkiv, “Probing the helium dimer by relativistic highly-charged projectiles,” (2021), arXiv:2105.02066 [physics.atom-ph].